PCCP

Accepted Manuscript

ROYAL SOCIETY OF CHEMISTRY

www.rsc.org/pccp

ARTICLE TYPE www. rsc.org/xxxxxx | XXXXXXXX

Identification of the dye adsorption modes in dye-sensitised solar cells with x-ray spectroscopy techniques: a computational study

Ali Akbari*[a], Javad Hashemi[a], Johannes Niskanen[a], Simo Huotari[a], and Mikko Hakala[a]

Received Xth XXXXXXXXXX 20XX, Accepted Xth XXXXXXXXX 20XX
First published on the web Xth XXXXXXXXXX 200X
DOI: 10.1039/b000000x

Adsorption geometry of dye molecules can have a substantial impact on the efficiency and functional lifespan of a dye-sensitised solar cell (DSSC) and therefore, its reliable assessment is an important step in engineering more efficient DSSCs. X-ray photoelectron spectroscopy (XPS) of oxygen is empirically proved to be the most efficient technique in distinguishing between the two most occurring adsorption geometries, i.e. monodentate and bidentate. In this computational study, we provide a comprehensive analysis of XPS and X-ray absorption spectroscopy (XAS) of carbon and oxygen for these binding modes in a perylene-sensitised TiO_2. We confirm that O 1s XPS has an excellent sensitivity in mode identification. Moreover, we show that the adsorption has a great impact on the XPS binding energies and reduces them by ~ 4 eV, and using this effect, we extend the XPS usage to study dye desorption in the cell. Finally, our results for XAS indicate that although less sensitive, the spectra from carbon can be used in mode detection.

1 Introduction

The present time is witnessing intensified global efforts to develop an efficient solar technology which is capable of competing with other energy resources. Among available candidates, dye sensitised solar cells (DSSCs)[1] offer a promising option for an inexpensive and efficient solar cell technology.

In a DSSC, the dye which is adsorbed on a semiconductor surface, typically TiO_2 nanoparticles, absorbs solar light and injects an electron into the semiconductor. Then, via a redox reaction with the solvent, the oxidized dye receives an electron and becomes regenerated. Due to the central role of the dye in this photon-current conversion, many attempts have been made to synthesize better dyes and push the efficiency to higher values. As a result, in the last two decades hundreds of different dyes have been synthesized,[2] ranging from ruthenium polypyridyl dyes[3–5] with their remarkable performance to inexpensive and environmentally friendly organic dyes.[6,7]

Another key factor in the efficiency of DSSCs is finding a proper functional group to bind the dye strongly to the oxide surface. The choice of the anchor group has direct consequences on the orientation and packing of adsorbed dyes on the semiconductor surface, affecting the rate and effectiveness of parasitic recombination reactions,[8,9] as well as the long-term stability of the cell.[10] The case of D5L2A1[11,12] and D5L2A3[13] dyes is a perfect example of such an influence where due to different anchoring units, the photovoltaic efficiency dropped severely from $\sim 6\%$ for D5L2A1[11,12] to $\sim 2\%$ in D5L2A3.[13]

Given this importance, numerous studies[8,10,13–38] have focused on the adsorption geometry of dye molecules and its effect on the cell efficiency. Currently, carboxylic acids are among the most used anchors due to their relative stability and easy synthesis.[2] They bind to the TiO2 surface from their COOH end in two main possible modes, monodentate and bidentate, which differ in the number of COOH oxygen atoms involved in the binding.[10] In the bidentate mode, the hydrogen in the COOH transfers to a nearby surface oxygen and then the oxygen atoms in the COO^- bind to either one (chelate) or two (bridging) surface Ti atoms. In contrast, in the monodentate, only one of the anchor oxygen atoms binds to a Ti (Fig. 1).

Many theoretical studies have shown that bidentate mode is the preferred mode of adsorption on rutile surfaces.[10,15,31,39] However, on anatase surfaces, despite the same general claim by Pastore *et al.*,[40] the results have shown that the binding mode depends on the carboxylic group utilized as the anchor,[28,31,32] the employed dye,[23,32,37,38,41,42] solvent effects,[27,32,34] and finally the method and the level of the theory involved in the simulations.[10,32,33,36,43]

At the experimental level, vibrational spectroscopy techniques such as Fourier Transform Infra-Red (FT-IR) spectroscopy and Surface-Enhance Raman Spectroscopy (SERS) have been commonly utilized to study the dye adsorption.[14,22] However, reliable mode identification with these techniques is only feasible for simple dyes and they face great difficulty for realistic dyes.[32,38] Another group of experimental techniques suitable for dye adsorption studies is core-level spectroscopy which has been used to gain detailed information on

[a] *Department of Physics, University of Helsinki, FI-00014, Helsinki, Finland. E-mail: ali.akbari@helsinki.fi*

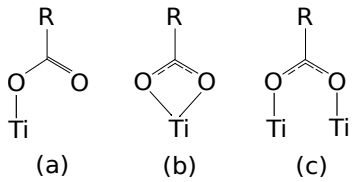

Fig. 1 Common possible binding modes for a carboxylate unit on TiO_2 surface: (a) monodentate (b) bidentate chelating (c) bidentate bridging. Here "R" denotes the rest of dye-anchor atoms.

the local structure, the relative orientation,[13,16,18,36] as well as the molecular and electronic structures of adsorbed dye molecules.[13,18,24,25,29,30]

Among x-ray techniques, X-ray photoelectron spectroscopy (XPS)[16,44–47] has been the method of choice for mode identification. The rationale behind this choice lies in the presence of different chemical bonds in these adsorption modes, i.e. in the bidentate modes, both of the anchor's oxygen atoms have bonds with the C and Ti (Fig. 1b and 1c), while in the monodentate, one bonds with C and Ti and the other with C and H (Fig. 1a). The assumption is that these different chemical bonds would lead to two different oxygen's XPS binding energies which are well-separated and detectable in the experiment. As a result, one expects to detect one less peak in the O 1s XPS spectra for the bidentate modes in comparison to the monodentate[16,44–47]. This intuitive picture, to the best of our knowledge, has been the only criterion used by experimentalists to asses the adsorption mode and no accurate XPS calculations have been performed to support it.

Hence, in this work we use a simple dye model system and include different binding modes (monodentate and bidentate) in the simulation to test this physical intuition. In addition to XPS, we also investigate computationally the capability and quality of X-ray absorption spectroscopy (XAS) in assessing the adsorption geometry. We examine O and C as the possible target elements for XAS and XPS and compare the sensitivity of each technique for mode identification. We confirm the excellent sensitivity of the XPS of O 1s for mode identification and show that XPS is superior to XAS in this regard. We also show that the adsorption onto the surface substantially reduces the XPS binding energies of the adsorbed dye with respect to the dye molecule. This suggests that this effect can be used to study and measure dye desorption in the cell.

2 Physical system and computational details

2.1 Model systems

To simulate a DSSC in our work, we chose a perylene-sensitised TiO_2 system. Perylene (Pe) dyes are well-known as chemically and photophysically stable dyes and have been

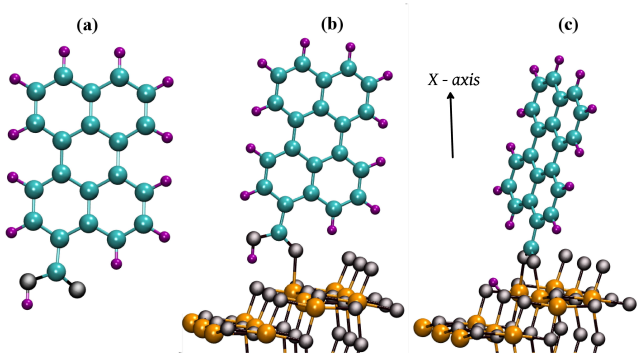

Fig. 2 H ▶ ●, C ▶ ●, O ▶ ●, Ti ▶ ●. Dye and dye-sensitised TiO_2 surface. (a) Perylene dye bearing COOH as the anchor (b) Monodentate adsorption of perylene onto TiO_2 surface (c) Bidentate adsorption.

used both experimentally[48,49] (reaching efficiency of $\sim 6\%$) and computationally[31,50]. In simulating the TiO_2 surface, we only considered the anatase (101) surface due to the fact that the DSSCs' fabrication processes produce anatase nanocrystals with (101) being the most abundant exposed plane[51]. Finally, COOH, the simplest carboxylic group, acts as an anchor and binds the Pe to the oxide surface.

Among the possible bindings modes (Fig.1), we disregard the bidentate chelating form from our study due to its rare occurrence[10,52] and examined the monodentate and bidentate bridging modes. To account for these binding modes in our calculations, we used the structures obtained by the work of Ikäläinen *et al.*[37]. These density-functional-theory-relaxed structures are two periodic supercells (192 atoms) comprising a four-layer TiO_2 with a perylene molecule adsorbed either bidentatedly (bridging) or monodentatedly. Although two forms for the monodentate were obtained by Ikäläinen *et al.*[37], they are very similar and we only focused on one of them (monodentate 2 in that reference). The cell dimensions were $35\mathring{A}$ in the x direction, with $11.35\mathring{A}$ and $10.24\mathring{A}$ in the y and z directions where the TiO_2 surface is in the y-z plane. Finally, for simulating Pe-COOH desorption from TiO_2, we used a large cubic box (nonperiodic simulation with the cell dimensions of $40\mathring{A}$) with the Pe-COOH molecule in its center. Fig. 2 shows our model systems.

2.2 Computational details

For core-level spectroscopy, we chose carbon and oxygen as the target elements and focused on the energy range required for exciting the 1s electrons*. The experimental spectra of

* The Ti atoms involve in the binding have the same type of bonds in the monodentate and bidentate (see Figs. 1a and 1c) and therefore, the changes in the Ti binding energies are expected to be very small. This intuition is backed by both the experimental results[53] and the result of our calculations for the

these elements can have contribution from the atoms in the anchor, the dye, and the titanium oxide surface and all these atoms should be taken into account in the simulation. However, in the case of oxygen spectra, the exact number depends on the penetration depth of the x-ray beam into the TiO_2 surface. Nonetheless, by considering only the oxygen atoms of the surface monolayer, we account for all the effects of the dye adsorption on the oxygen spectra (after one monolayer, the oxygen atoms regain essentially their bulk profile, adding a constant background to the total spectra). Considering our simulation cells, we included 21 carbon atoms (20 for Pe and 1 for the anchor) and 26 oxygen atoms (24 for the surface monolayer and 2 for the anchor) for the carbon and oxygen spectra in the calculations respectively. Finally, we note that due to the random orientation of the TiO_2 nanocrystals in DSSCs, the observed XAS spectra are the spherical average of all possible orientations.

To predict the outcome of XAS and XPS, we use the density functional theory (DFT)[54] at the level of PBE exchange-correlation functional[55]. In this framework, we calculate the result of XAS experiments with the help of the half-core-hole transition potential approximation (TPA)[56], which is an approximation to account for the relaxation effects[57] in DFT. We also perform a ΔSCF calculation for the first excitation energy to align the corresponding absorption spectrum and decrease the errors introduced by TPA. The simulation of XPS is more straightforward and is done by calculating the energy difference between the ionized system (removing one electron from the core of the target atom) and the neutral system. It is worth mentioning that we do not account for the effect of vibronic coupling on the spectrum in our calculations. Such a coupling can produce fine vibrational structure where each peak is replaced by several equidistant progressive peaks starting from the original peak (the distance is equal to the corresponding vibration frequency). While these effects can in principle be calculated[58–61], the enormous increase in their computational cost for our systems makes them impractical.

We carried out all the calculations with the CP2K code,[62] which is based on the Gaussian augmented plane wave "GAPW" formalism[63–65†]. In all calculations we used an all-electron representation of the excited atom by the very large and highly accurate aug-cc-pV5Z basis set[66]. The cutoff energy is set to 400 Ry to converge the energy. Moreover, for a converged XAS spectra in the energy range shown in this work, we included 500 unoccupied orbitals in the calculation. Finally, to ensure a sound comparison between the nonperiodic calculation of Pe-COOH and the periodic calculations, we also used the same periodic cell but with ghost orbitals for the TiO_2 surface; the results were essentially identical to the nonperiodic calculation. This also shows that the intercell interactions between dyes are negligible in our systems.

2.3 Broadening schemes

The spectra in a real experiment is the result of many interactions which some of them are not included in our ab-initio treatment. To predict the experimental spectra, we must convolute the calculated spectra with a proper broadening to incorporate approximately the effect of these ignored interactions. Usually, one only needs to account for the experimental resolution and the core-hole life time. However, the neglected vibronic coupling in our calculations can introduce a dominant extra broadening (experimentally, these couplings can lead to an asymmetrical Gaussian broadening of our peaks where the level of asymmetries are deducted from the experimental spectra). As a result, in predicting the experimental situation and for a more comprehensive comparison, we consider the following broadening schemes.

- *Scheme I*. Assuming no vibrational fine structure in the spectra, we only take into account the broadening due to the fundamental life time and the instrument resolution and apply a Lorentzian (C 1s: FWHM=0.1 eV, O 1s=0.15 eV)[67] and Gaussian (FWHM=0.1 eV for a very accurate instrument) broadening to the calculated spectra.
- *Scheme II*. To approximate the effect of vibrational fine structure for a rather strong vibronic coupling, we ignore the asymmetry and apply a wide Gaussian broadening (FWHM = 0.9 eV) to each peak of the spectra.

Using these two schemes, we will compare our results with the experimental spectra of similar systems and estimate qualitatively the strength of these interactions.

3 Results and discussions

Before presenting the results, we note here that due to the approximations made in ab-initio calculations and model systems, the absolute energy values obtained in the simulation can have a shift with respect to the experiment. Therefore, it

2p XPS binding energies. Our calculations showed that in the bidentate, all the Ti atoms have the same binding energies (less than 0.05 eV difference). As for the monodentate mode, the largest observed difference was 0.2 eV and corresponds to the Ti atom directly bonded to the dye; the other Ti atoms of the TiO2 surface had essentially equal binding energies (similar to the bidentate mode, i.e. less than 0.05 eV difference between each other). Considering the broadening present in experiment, these differences are too small to be used for mode identification.

† Technical note for CP2K code: Throughout this work we noticed that it is *crucial* to modify the default values for the CP2K parameters "LEBEDEV GRID" (between 50 and 80) and "RADIAL GRID" (between 100 and 200) and set the density and energy convergence in the order of 5×10^{-8} and 5×10^{-10} Ha (or even better) respectively in the core-level part of the calculation. Based on our observations, in particular in the case of XPS simulations, some of the converged energies in a less stricter criterion ($\Delta E \sim 10^{-7}$ Ha) can change substantially (~ 2 eV).

Table 1 Calculated C 1s XPS binding energies (E_b) of anatase (101) surface sensitised with Pe-COOH in the monodentate and the bidentate adsorption modes. Here "A" and "P" denote the anchor and perylene.

Excited C	E_b^{1s} (eV)
Pe-COOH	
C_A	292.2
C_P	[288.8-289.7]
Monodentatedly adsorbed dye	
C_A	$\sim 288^{\dagger}$
C_P	[284-285]
Bidentatedly adsorbed dye	
C_A	287.8
C_P	[284.1-285.1]

†Not fully converged.

Table 2 Calculated O 1s XPS binding energies (E_b) of anatase (101) surface sensitised with Pe-COOH in the monodentate and the bidentate adsorption modes. Here "A", "S", and "H" denote the anchor, the surface, and the transferred hydrogen to the surface with "-" showing their bonding.

Excited O	E_b^{1s} (eV)	$\Delta = E_b^{1s}$ - 530 (eV)
O_S	[530-530.5]	[0-0.5]
Monodentatedly adsorbed dye		
$O_{A\text{-}S}$	531.4	1.4
O_A	532.8	2.8
Bidentatedly adsorbed dye		
$O_{A\text{-}S}$	531.2	1.2
$O_{S\text{-}H}$	531.6	1.6
Pe-COOH		
$O_{A(C\text{-}O)}$	535.2	5.2
$O_{A(C\text{-}O\text{-}H)}$	537.6	7.6

is more meaningful to focus on the respective positions of the peaks in spectra.

3.1 XPS

The binding energies are given in Tables 1 and 2 and the corresponding XPS spectra are plotted in Fig. 3. We now examine the results and discuss the sensitivity of the carbon and oxygen spectra to the binding modes.

Carbon. As Table 1 shows, the carbon atoms of perylene in the gas phase have the binding energy in the range $[288.8 - 289.7]$eV. Upon adsorption, this energy range changes to $[284 - 285]$eV in the monodentate binding mode and $[284.1 - 285.1]$eV in the bidentate mode. The XPS value for the anchor also decreases from 292.3 eV to 287.8 in the monodentate (the result for the bidentate did not fully converge although the value is close to 288 eV). Therefore, the dye adsorption substantially reduces the binding energy of the carbon 1s electrons by ~ 4.5 eV. Such a significant shift enables us to spot the dye detachment from the surface where the ratio between them estimates the percentage of desorbed dyes. As for the mode identification, the existing 0.1 eV difference between monodentate and bidentate is likely to be too small to be used for this purpose.

Oxygen. In the case of XPS of the oxygen atoms, most of the XPS signal in the experiment would come from the TiO_2 surface (O_S) and produce the main peak in the XPS experiment. Therefore, they can act as the reference point around which we search for the fingerprints of the adsorption geometry and dye detachment. Based on our calculations, the binding energies of O_S are distributed in energy interval of [530-530.5]eV, in good agreement with the experimental results[24]. From this range we choose the reference point to be at 530 eV and measure the other binding energies with respect to it. We present the results in Table 2.

Analogous to the XPS of carbon, the signal from the anchor is well separated from the rest of the system (here, the surface) and there are significant differences between the monodentate, bidentate, and the desorbed dye. As expected, in the bidentate, both oxygen atoms of the anchor $O_{A\text{-}S}$ have equal XPS energies (1.2 eV with respect to the surface) while in the monodentate, they differ by 1.4 eV (1.4 for the binding oxygen $O_{A\text{-}S}$ and 2.8 eV for the other O_A). Hence, if one detects an XPS signal blue shifted by 2.8 eV, the binding geometry is monodentate; otherwise, the adsorption takes the bidentate geometry. Moreover, an isolated Pe-COOH shows two XPS signals in the energy range of [5-8]eV with respect to the surface oxygen (5.2 eV and 7.6 eV) and can be used to detect the presence of detached dyes in the system.

Comparing the results of XPS from C and O, we see that the XPS measurement of oxygen is more sensitive to mode detection compared with carbon. The results also reveals that the adsorption substantially reduces the binding energies of 1s electrons (approximately by 4 eV) with respect to the isolated Pe-COOH. Examining the C-C and C-H bond lengths between the isolated and the adsorbed Pe did not reveal any bond-length changes upon adsorption. Therefore, such a significant change in the XPS binding energies can be due to charge redistribution in the dye-TiO_2 system and is in contrast with the notion that only the local chemical bonds determine the binding energy. To support this claim we performed Mulliken charge analysis[68] for both the ground state and the core-excited state (via Z+1-approximation[69]) of the isolated dye and dye-adsorbed systems. Examining the net charge of the excited atoms of the dye (carbon or oxygen) and the atoms directly bonded to them, we observed essentially no change be-

tween the adsorbed and isolated systems (neither in the ground nor in the core-excited state). This will rule out the role of local effects in the strong binding energy shifts. However in a bigger picture, we observed a surface-to-dye charge transfer in the excited dye-adsorbed system with respect to its ground state. Therefore, although we could not pinpoint the exact relation, the global charge redistribution that can be correlated to the strong binding energy shift.

Additionally, it is worth mentioning that the dye adsorption also decreases the energy difference between the oxygen atoms of the anchor, i.e. the difference of 2.4 eV in Pe-COOH reduces to 1.4 eV in monodentate. This suggests that it is possible that for other dye-anchors, the difference becomes comparable with the broadening present in the experiment and therefore can make the mode identification difficult.

Finally, to connect our calculations to the experiment, we can use the calculated XPS binding energies and predict the corresponding XPS spectra. While our XPS calculations do not provide the corresponding intensities, due to the very localized nature of the 1s orbital, we can assume that all the atoms of the same element have equal intensities. With this assumption and using the two broadening schemes (see Sec. 2.3), we have plotted the XPS spectra in Fig. 3. The figure clearly shows that compared with carbon (Figs. 3a and 3b), the XPS measurement of oxygen is much more sensitive to the adsorption mode and has distinctive features in both schemes (Figs. 3c and 3d). Comparing our results with the existing experiments for different dyes [16,44–47] shows that their O 1s XPS spectra are very similar to Fig. 3d in which the presence of the pronounced shoulder without the additional peak has been interpreted as the fingerprint of the bidentate mode. As for the C 1s XPS spectra, the experimental spectra for a similar perylene dye [53] are very comparable to Fig. 3b, and apart from a constant shift, our spectra are in a good agreement with the experiment. [53]

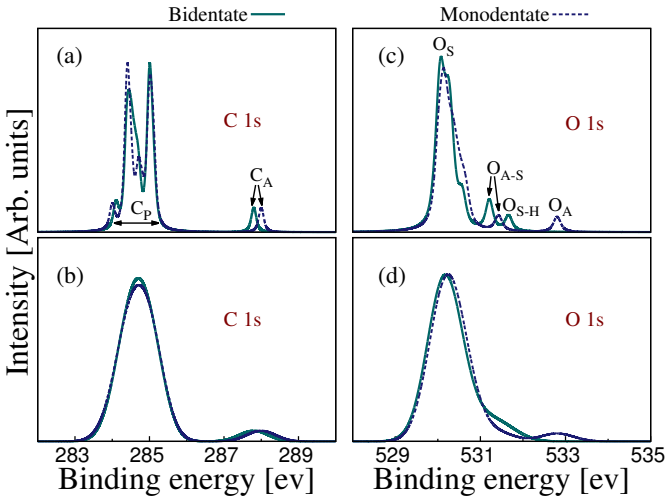

Fig. 3 Calculated C 1s and O 1s XPS spectra of Pe-COOH adsorbed on anatase (101) in the monodentate and the bidentate binding modes. To produce the spectra, the data in Tables 1 and 2 were used and the contribution of the atoms below the surface monolayer was ignored. In (a) and (c), the broadening scheme I was used while (b) and (d) are broadened with the scheme II (see Sec. 2.3).

3.2 XAS

We present the calculated K-edge x-ray absorption spectra of carbon and oxygen in Fig. 4 for two different broadening schemes. In the following we compare the spectral features of each element in different binding modes and then briefly discuss on the dye desorption.

Carbon. In the case of the carbon spectra (Figs. 4a and 4b), both of the spectra show identical behaviour up to $\sim$ 284.2 eV in the broadening scheme I or $\sim$ 285.5 eV in the scheme II. Then, the bidentate mode in the scheme I (Fig. 4a) exhibits two sharp peaks at $\sim$ 284.5 eV and $\sim$ 285 eV compared to one peak $\sim$ 284.8 eV for the monodentate. Another noticeable difference in this scheme occurs in the range [286.6-289.6]eV where the bidentate has four peaks visible at $\sim$ 287 eV, $\sim$ 287.5 eV, $\sim$ 288.3, and $\sim$ 288.5 in compari-

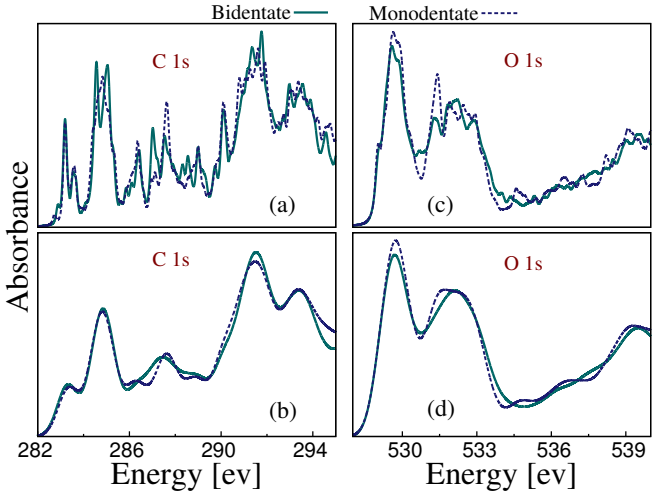

Fig. 4 Spherically averaged C and O K-edge XAS spectra of an anatase (101) sensitised with Pe-COOH in the bidentate and the monodentate binding modes. The broadening scheme I was used in (a) and (c) and the scheme II in (b) and (d) (see Sec. 2.3). In (c) and (d), the contribution from the surface oxygen atoms is limited to the outermost surface monolayer.

son to the very sharp peak of the monodentate at $\sim$ 287.6 eV. In the scheme II (Fig. 4b), compared to the bidentate mode which has one pronounced peak at $\sim$ 287.5 eV, the monodentate mode produces three pronounced peaks at $\sim$ 286.2 eV, $\sim$ 287.6 eV, and $\sim$ 289 eV.

Oxygen. As for the oxygen, the XAS spectra in the scheme II (Fig. 4) do not show distinctive features useful for mode identification and only the scheme I (Fig. 4c) keeps the possibility open. In this scheme, there is a significant increase in the absorption at $\sim$ 532.1 eV for monodentate which offers a way to identify the binding mode. However, the difference in the absorption at this energy mainly originates from the surface oxygen atoms. The closer inspection pinpoints, although we have not shown it here, that this difference is only caused by the adsorption of a hydrogen atom onto the surface in the bidentate adsorption mode (see Fig. 2). Considering that we only accounted for the oxygen atoms of one monolayer and the presence of contaminations in any experiment, this suggests that any mode detection via XAS of oxygen atom is very difficult.

At the experimental level, the existing results of different dyes show that the C K-edge XAS spectra depend on the dye and its binding geometry strongly,[47,53,70] and a direct comparison to our results is not possible. In the case of oxygen, the shape of spectra in Fig. 4d is similar to the experiment for a DSSC with N-719 as the dye[70]. Nevertheless, all these experiments[47,53,70] show that broadening with the scheme II is more realistic and therefore, the vibronic coupling must be quite strong.

Finally, our calculations showed that the XAS is insensitive to dye desorption. This is due to the fact that the Pe-COOH molecules absorb x-ray photons in the same energy range as the adsorbed dyes, and therefore, in a XAS experiment, their spectra will be buried by the spectra of the adsorbed dyes and not detectable.

4 Conclusions

In this work we studied a DSSC model system (perylene-sensitised TiO_2) and examined in detail the applicability of two x-ray spectroscopy techniques for such a purpose. We confirmed the excellent sensitivity of the O 1s XPS spectra in mode detection and showed that the K-edge XAS spectra of carbon can also have the fingerprints of the adsorption mode. However, compare to the XPS, the XAS spectra do not have a universal feature for detecting the binding mode and ab-initio calculations are always needed to interpret the spectra. Furthermore, we demonstrated that the adsorption has a considerable effect on the XPS binding energies and suggested that this effect can be used to study dye desorption. In contrast, the XAS spectra is unlikely to provide useful information about the dye desorption in the system. All these results show that XPS spectroscopy, in particular of oxygen, is superior to XAS in detecting the adsorption mode and the dye desorption.

5 Acknowledgement

This work has been supported by the Academy of Finland (contract numbers 1259599, 1260204, 1254065,1283136, and 1259526). We also acknowledge CSC, IT Center for Science, for granting generous computational resources. We thank Dr. S. Ikäläinen and Professor K. Laasonen for providing the structure of the systems studied in this work. We would also like to thank A. Musazay for many fruitful discussions during this project.

References

1 B. O'Regan and M. Grätzel, *Nature*, 1991, **353**, 737–740.
2 P. H., A. Hagfeldt, G. Boschloo, L. Sun, L. Kloo and H. Pettersson, *Chem. Rev.*, 2010, **110**, 6595.
3 M. K. Nazeeruddin, A. Kay, I. Rodicio, R. Humphry-Baker, E. Mueller, P. Liska, N. Vlachopoulos and M. Graetzel, *Journal of the American Chemical Society*, 1993, **115**, 6382–6390.
4 M. K. Nazeeruddin, F. De Angelis, S. Fantacci, A. Selloni, G. Viscardi, P. Liska, S. Ito, B. Takeru and M. Grätzel, *Journal of the American Chemical Society*, 2005, **127**, 16835–16847.
5 M. K. Nazeeruddin, P. Pechy and M. Gratzel, *Chem. Commun.*, 1997, 1705–1706.
6 B. P., *Angew. Chem., Int. Ed.*, 2009, **48**, 2474.
7 W. Zeng, Y. Cao, Y. Bai, Y. Wang, Y. Shi, M. Zhang, F. Wang, C. Pan and P. Wang, *Chemistry of Materials*, 2010, **22**, 1915–1925.
8 N. Martsinovich, D. R. Jones and A. Troisi, *The Journal of Physical Chemistry C*, 2010, **114**, 22659–22670.
9 N. Martsinovich and A. Troisi, *The Journal of Physical Chemistry C*, 2011, **115**, 11781–11792.
10 A. Vittadini, A. Selloni, F. P. Rotzinger and M. Grätzel, *The Journal of Physical Chemistry B*, 2000, **104**, 1300–1306.
11 D. P. Hagberg, T. Edvinsson, T. Marinado, G. Boschloo, A. Hagfeldt and L. Sun, *Chem. Commun.*, 2006, 2245–2247.
12 D. P. Hagberg, J.-H. Yum, H. Lee, F. De Angelis, T. Marinado, K. M. Karlsson, R. Humphry-Baker, L. Sun, A. Hagfeldt, M. Grätzel and M. K. Nazeeruddin, *Journal of the American Chemical Society*, 2008, **130**, 6259–6266.
13 T. Marinado, D. P. Hagberg, M. Hedlund, T. Edvinsson, E. M. J. Johansson, G. Boschloo, H. k. Rensmo, T. Brinck, L. Sun and A. Hagfeldt, *Physical chemistry chemical physics : PCCP*, 2009, **11**, 133–41.
14 K. S. Finnie, J. R. Bartlett and J. L. Woolfrey, *Langmuir*, 1998, **14**, 2744–2749.
15 S. Bates, G. Kresse and M. Gillan, *Surface Science*, 1998, **409**, 336–349.
16 A. Thomas, W. Flavell, C. Chatwin, S. Rayner, D. Tsoutsou, A. Kumarasinghe, D. Brete, T. Johal, S. Patel and J. Purton, *Surface Science*, 2005, **592**, 159–168.
17 C. Pérez León, L. Kador, B. Peng and M. Thelakkat, *The journal of physical chemistry. B*, 2006, **110**, 8723–30.
18 E. Johansson, T. Edvinsson, M. Odelius, D. Hagberg, L. Sun, A. Hagfeldt, H. Siegbahn and H. Rensmo, *Journal of Physical Chemistry C*, 2007, **111**, 8580–8586.
19 F. Labat and C. Adamo, *The Journal of Physical Chemistry C*, 2007, **111**, 15034–15042.

20 W. H. Howie, F. Claeyssens, H. Miura and L. M. Peter, *Journal of the American Chemical Society*, 2008, **130**, 1367–1375.

21 D. Rocca, R. Gebauer, F. De Angelis, M. K. Nazeeruddin and S. Baroni, *Chemical Physics Letters*, 2009, **475**, 49–53.

22 K. Srinivas, K. Yesudas, K. Bhanuprakash, V. J. Rao and L. Giribabu, *The Journal of Physical Chemistry C*, 2009, **113**, 20117–20126.

23 F. De Angelis, S. Fantacci, A. Selloni, M. K. Nazeeruddin and M. Gratzel, *The Journal of Physical Chemistry C*, 2010, **114**, 6054–6061.

24 S. Yu, S. Ahmadi, M. Zuleta, H. Tian, K. Schulte, A. Pietzsch, F. Hennies, J. Weissenrieder, X. Yang and M. Göthelid, *The Journal of chemical physics*, 2010, **133**, 224704.

25 M. Hahlin, E. M. J. Johansson, S. Plogmaker, M. Odelius, D. P. Hagberg, L. Sun, H. Siegbahn and H. k. Rensmo, *Physical chemistry chemical physics : PCCP*, 2010, **12**, 1507–17.

26 K. E. Lee, M. A. Gomez, S. Elouatik and G. P. Demopoulos, *Langmuir : the ACS journal of surfaces and colloids*, 2010, **26**, 9575–83.

27 F. De Angelis, S. Fantacci and R. Gebauer, *The Journal of Physical Chemistry Letters*, 2011, **2**, 813–817.

28 R. Luschtinetz, S. Gemming and G. Seifert, *The European Physical Journal Plus*, 2011, **126**, 98.

29 K. M. Karlsson, X. Jiang, S. K. Eriksson, E. Gabrielsson, H. k. Rensmo, A. Hagfeldt and L. Sun, *Chemistry (Weinheim an der Bergstrasse, Germany)*, 2011, **17**, 6415–24.

30 M. Hahlin, E. M. J. Johansson, R. Scholin, H. Siegbahn and H. Rensmo, *The Journal of Physical Chemistry C*, 2011, **115**, 11996–12004.

31 F. Ambrosio, N. Martsinovich and A. Troisi, *The Journal of Physical Chemistry Letters*, 2012, **3**, 1531–1535.

32 C. Anselmi, E. Mosconi, M. Pastore, E. Ronca and F. De Angelis, *Physical chemistry chemical physics : PCCP*, 2012, **14**, 15963–74.

33 M. Pastore and F. De Angelis, *Physical chemistry chemical physics : PCCP*, 2012, **14**, 920–8.

34 E. Mosconi, A. Selloni and F. De Angelis, *The Journal of Physical Chemistry C*, 2012, **116**, 5932–5940.

35 S. Manzhos, H. Segawa and K. Yamashita, *Physical chemistry chemical physics : PCCP*, 2012, **14**, 1749–55.

36 T. P. Brennan, J. T. Tanskanen, J. R. Bakke, W. H. Nguyen, D. Nordlund, M. F. Toney, M. D. McGehee, A. Sellinger and S. F. Bent, *Chemistry of Materials*, 2013, **25**, 4354–4363.

37 S. Ikäläinen and K. Laasonen, *Physical chemistry chemical physics*, 2013, **15**, 11673–8.

38 J. Calbo, M. Pastore, E. Mosconi, E. Ortí and F. De Angelis, *Physical chemistry chemical physics : PCCP*, 2014, **16**, 4709–19.

39 U. Diebold, *Surface Science Reports*, 2003, **48**, 53–229.

40 M. Pastore, S. Fantacci and F. De Angelis, *The Journal of Physical Chemistry C*, 2013, **117**, 3685–3700.

41 F. Schiffmann, J. VandeVondele, J. Hutter, R. Wirz, A. Urakawa and A. Baiker, *The Journal of Physical Chemistry C*, 2010, **114**, 8398–8404.

42 Y. Jiao, F. Zhang, M. Grätzel and S. Meng, *Advanced Functional Materials*, 2013, **23**, 424–429.

43 F. Nunzi and F. De Angelis, *The Journal of Physical Chemistry C*, 2011, **115**, 2179–2186.

44 L. Patthey, H. Rensmo, P. Persson, K. Westermark, L. Vayssieres, A. Stashans, A. Petersson, P. A. Bruhwiler, H. Siegbahn, S. Lunell and N. MaŁrtensson, *The Journal of Chemical Physics*, 1999, **110**, 5913.

45 J. Schnadt, A. Henningsson, M. P. Andersson, P. G. Karlsson, P. Uvdal, H. Siegbahn, P. A. Brühwiler and A. Sandell, *The Journal of Physical Chemistry B*, 2004, **108**, 3114–3122.

46 E. M. J. Johansson, S. Plogmaker, L. E. Walle, R. Scholin, A. Borg, A. Sandell and H. Rensmo, *The Journal of Physical Chemistry C*, 2010, **114**, 15015–15020.

47 K. L. Syres, A. G. Thomas, W. R. Flavell, B. F. Spencer, F. Bondino, M. Malvestuto, A. Preobrajenski and M. Grätzel, *The Journal of Physical Chemistry C*, 2012, **116**, 23515–23525.

48 M. Planells, F. J. Cespedes-Guirao, A. Forneli, A. Sastre-Santos, F. Fernandez-Lazaro and E. Palomares, *J. Mater. Chem.*, 2008, **18**, 5802–5808.

49 U. B. Cappel, M. H. Karlsson, N. G. Pschirer, F. Eickemeyer, J. Schoneboom, P. Erk, G. Boschloo and A. Hagfeldt, *The Journal of Physical Chemistry C*, 2009, **113**, 14595–14597.

50 P. Persson, M. J. Lundqvist, R. Ernstorfer, W. A. Goddard and F. Willig, *Journal of Chemical Theory and Computation*, 2006, **2**, 441–451.

51 M. Lazzeri, A. Vittadini and A. Selloni, *Physical Review B*, 2001, **63**, 155409.

52 M. Pastore and F. D. Angelis, *ACS nano*, 2010, **4**, 556–62.

53 L. Cao, Y. Wang, J. Zhong, Y. Han, W. Zhang, X. Yu, F. Xu, D.-C. Qi and A. T. S. Wee, *The Journal of Physical Chemistry C*, 2011, **115**, 24880–24887.

54 W. Kohn and L. J. Sham, *Phys. Rev.*, 1965, **140**, A1133—-A1138.

55 J. P. Perdew, K. Burke and M. Ernzerhof, *Phys. Rev. Lett.*, 1996, **77**, 3865–3868.

56 J. C. Slater and K. H. Johnson, *Phys. Rev. B*, 1972, **5**, 844–853.

57 L. Triguero and L. G. M. Pettersson, *Physical Review B*, 1998, **58**, 8097–8110.

58 I. Minkov, F. Gel'mukhanov, R. Friedlein, W. Osikowicz, C. Suess, G. Ohrwall, S. L. Sorensen, S. Braun, R. Murdey, W. R. Salaneck and H. Agren, *The Journal of chemical physics*, 2004, **121**, 5733–9.

59 U. Hergenhahn, *Journal of Physics B: Atomic, Molecular and Optical Physics*, 2004, **37**, R89–R135.

60 I. Minkov, F. Gel'mukhanov, H. Agren, R. Friedlein, C. Suess and W. R. Salaneck, *The journal of physical chemistry. A*, 2005, **109**, 1330–6.

61 W. Hua, J. D. Biggs, Y. Zhang, D. Healion, H. Ren and S. Mukamel, *Journal of chemical theory and computation*, 2013, **9**, 5479–5489.

62 J. Hutter, M. Iannuzzi, F. Schiffmann and J. VandeVondele, *Wiley Interdisciplinary Reviews: Computational Molecular Science*, 2014, **4**, 15–25.

63 G. Lippert, J. Hutter and M. Parrinello, *Theor. Chem. Acc.*, 1999, **103**, 124–140.

64 J. VandeVondele, M. Krack, F. Mohamed, M. Parrinello, T. Chassaing and J. Hutter, *Computer Physics Communications*, 2005, **167**, 103–128.

65 M. Iannuzzi and J. Hutter, *Physical chemistry chemical physics : PCCP*, 2007, **9**, 1599–610.

66 T. H. Dunning, *J. Chem. Phys.*, 1989, **90**, 1007–1023.

67 J. L. Campbell and T. Papp, *X-Ray Spectrometry*, 1995, **24**, 307–319.

68 R. S. Mulliken, *The Journal of Chemical Physics*, 1955, **23**, 1833–1840.

69 P. A. Lee and G. Beni, *Phys. Rev. B*, 1977, **15**, 2862–2883.

70 K. E. Lee, M. A. Gomez, T. Regier, Y. Hu and G. P. Demopoulos, *The Journal of Physical Chemistry C*, 2011, **115**, 5692–5707.